Dust and Gas in NGC3627

Dust and Gas in NGC3627 Using Observations from SCUBA-2

By

Jonathan H. Newton, B.A.

A Thesis

Submitted to the School of Graduate Studies

in Partial Fulfilment of the Requirements

for the Degree

Master of Science

McMaster University

Master of Science (2014) McMaster University

(Physics and Astronomy) Hamilton, Ontario

TITLE: Dust and Gas in NGC3627 Using Observations from SCUBA-2

AUTHOR: Jonathan Newton, B.A. (Western Kentucky University)

SUPERVISOR: Christine D. Wilson

NUMBER OF PAGES: x, 65

Abstract

Saw some dust and wanted to do something about it!

To my family and Poly.

Acknowledgements

When life looks like easy street, there is danger at your door... -Robert Hunter

Thank Chris and group members of course. Don't forget Christian!

Table of Contents

List of Figures

List of Tables

Chapter 1

Spectral Energy Distribution Analysis

1.1 SED Fitting Method

In order to determine a dust mass, we use the IDL package MPFIT (Markwardt, 2009) to fit equation 3.1 for the temperature, T, mass, M, and the emissivity index, β. The routine MPFIT utilizes the Levenberg-Marquardt algorithm. This algorithm uses a combination of two minimization techniques (the steepest descent method and the Newton-Raphson Method) to determine the parameter combination that corresponds to a minimum in the χ^2 space while maximizing the efficiency of the step sizes in each iteration (Burden & Faires, 2001). The algorithm begins by implementing the steepest descent method. This working of this technique is to follow the direction opposite of the largest gradient in order to traverse the χ^2 space to locate a minimum. As the set of solutions approaches a minimum, it will switch to the Newton-Raphson method to locate the best set of parameters by finding where the derivative at that point is closest to zero (Gavin, 2013).

Table 1.1. Calibration Factors for SCUBA-2 and KINGFISH Observations

Observation	Scaling Factor
100μm	0.03
160μm	0.05
250μm	0.07
350μm	0.07
450μm	0.12
500μm	0.07
850μm	0.08

$$S_\nu(T) = \frac{M\,\kappa_{\nu,0}}{D^2}\left(\frac{\nu}{\nu_0}\right)^{\beta+3} B_\nu(T) \tag{1.1}$$

In order for MPFIT to provide the most accurate fit, we establish a reasonable error for each of our data points, and determine a realistic set of starting points for the fitting. The variance for our SCUBA-2 data is determined by equation 3.2 such that σ_{obs} is the noise determined by MAKEMAP, $\sigma_{rms,sky}$ is the RMS of the sky, and σ_{calib} is the calibration uncertainties where the scaling factor is shown in table 3.1.

$$\sigma^2 = \sigma_{obs}^2 + \sigma_{rms,sky}^2 + \sigma_{calib}^2 \tag{1.2}$$

The variance for the KINGFISH data are determined in a similar fashion and are shown in equation 3.3, however the observation error is excluded since the reported variance in the filtered images are reflective of the fake source image used and not of the KINGFISH data set.

$$\sigma^2 = \sigma^2_{rms,sky} + \sigma^2_{calib} \tag{1.3}$$

The nature of the Levinberg-Marquardt method leaves the solution vulnerable to converge at a local minimum rather than converging at the global minimum. This is remedied by selecting reasonable initial conditions. The initial conditions we used were a modified blackbody with a temperature of 20K, a dust emissivity index of 2, and a mass determined by equation 3.4 using the flux from the 250μm emission and our initial temperature and dust emissivity values.

$$\begin{aligned} M &= \frac{D^2\, I_{250}}{\kappa_{\nu,0}\, B_{250}\,(T)} \left(\frac{\nu}{\nu_0}\right)^{-(\beta+3)} \\ &= 2.24 \times 10^5\, I_{250}\ \ [M_\odot] \end{aligned} \tag{1.4}$$

1.2 Fitting the Spectral Energy Distribution

The fitting procedure was carried out in two different ways on a modified blackbody equation, equation 3.1. One of the two methods is fitting an SED to each individual pixel in order to generate a set of parameter maps, and the second is by totaling the flux of each of the selected regions shown in figure 3.1 to maximize the signal to noise ratio in order to generate a more precise set of parameters. For both of the fitting methods the mass, M, and temperature, T, are set as free parameters, but the treatment of the emissivity index, β, required special treatment for each of the methods. The distance, D, has been set to 9.4 Mpc (Walter et al., 2008), and the reference opacity,

$\kappa_{\nu,0}$, was tested using 0.2665 m^2 kg$-$1 (Li & Draine, 2001) and 1.0 m$^-$2 kg$^-$1 (Planck Collaboration et al., 2011).

1.2.1 Pixel SED Fits

In order to generate a parameter map of NGC3627, each individual pixel has it's own SED determined from the available wavelengths described in the observations chapter. Initially, we exclude the 500μm emission, and in later fits, we substitute the 450μm emission with 500μm emission. The treatment of the dust emissivity index is performed by fixing it at $\beta = 1.8$ for the Planck opacity model such that the opacity is $\kappa_{300\mu m,0} = 1.0$ m^2 kg^{-1} (Planck Collaboration et al., 2011) and $\beta = 2.0$ for the Li and Draine opacity model where the opacity is $\kappa_{300\mu m,0} = 0.2665$ m^2 kg^{-1} (Li & Draine, 2001). A third fit is performed where the emissivity index is allowed to vary as a free parameter. While the emissivity index is allowed to vary, the opacity being used is the Planck model in order to generate a minimum mass estimate of the two opacity values. Using either an opacity of 1.0 m^2 kg^{-1} or 0.2665 m^2 kg^{-1} will not effect the shape of the SED, only the its normalizing value. In the case of our fits, it is the mass that acts as the normalizing constant, so increasing or decreasing the opacity will yield the opposite effect in the mass. The inverse proportionality can be seen in equation 3.4. The resulting parameter maps of the fits are shown in figure 3.2. The numerical values from fitting each model are shown in tables 3.2, 3.3, and 3.4 where each region corresponds to the regions labeled in figure 3.1.

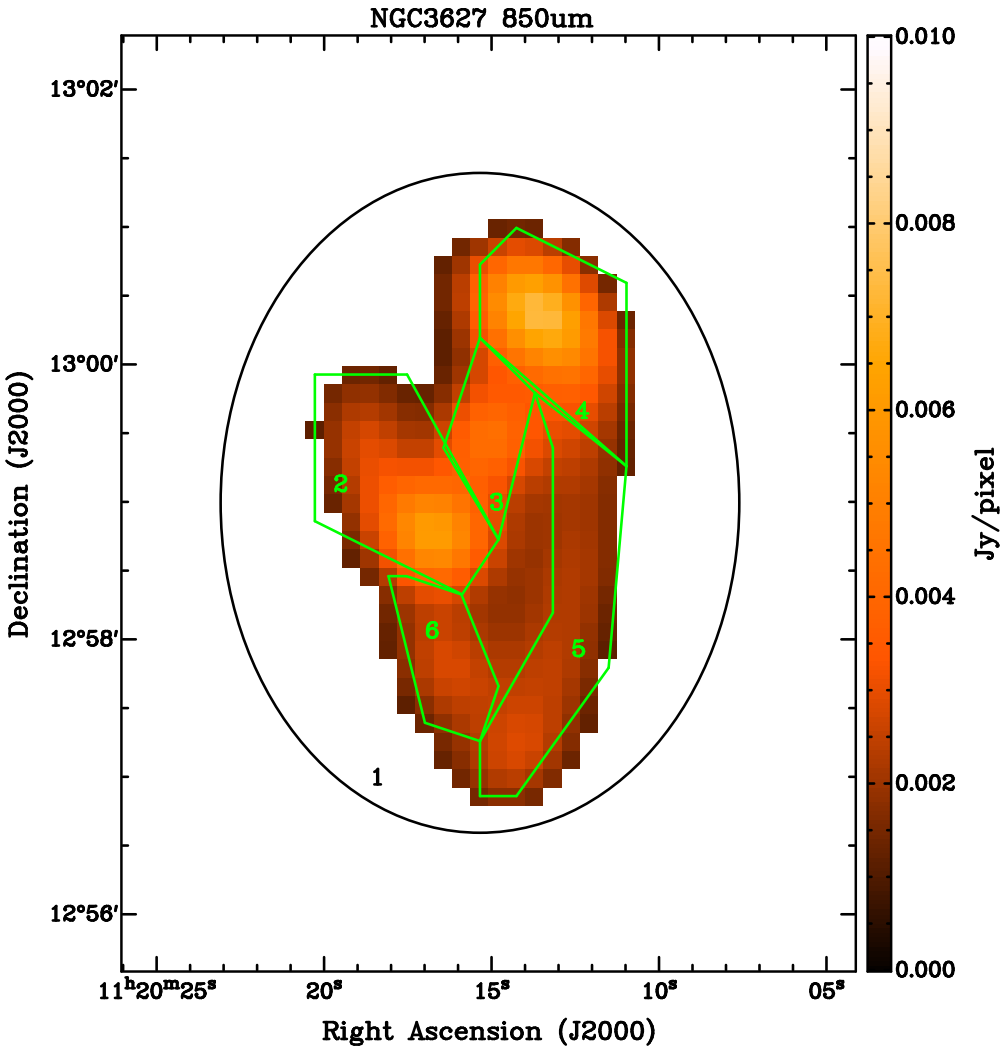

Figure 1.1: 850μm emission convolved to the 500μm beam size overlaid with the selected regions of NGC3627 labeled 1 through 6 such that region 1 includes the entire galaxy.

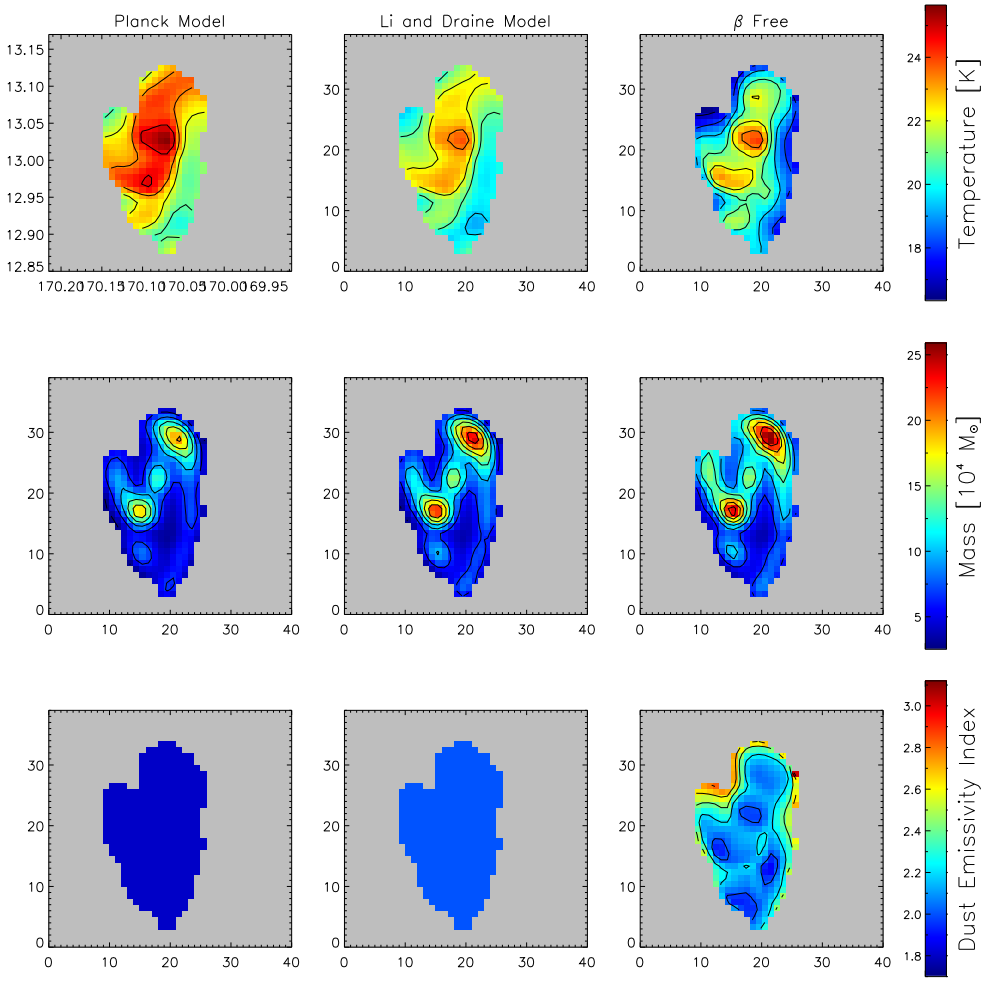

Figure 1.2: Returned value for the SED fits with the Planck model in the left column, the Li and Draine model in the middle column, and β as a free variable in the right column. The top row shows the temperature with contours from 1.5K to 28.5K in 1.5K increments. The second row show the returned masses with contours from $1.9M_{\odot}$ to $13.3M_{\odot}$ in $1.9M_{\odot}$ increments. The Li and Draine mass fits have been divided by three to better show the features. Th bottom row shows the returned dust emissivity index values with contours from 1.8 to 2.8 with 0.2 increments.

Table 1.2. Best Fit Parameters for Planck Model

Region	Average β	Total Mass $[10^5 M_\odot]$	Surface Density $[M_\odot pc^{-2}]$	Average Temperature [K]
1	1.8	47 ± 22	0.09 ± 0.04	26 ± 2
2	1.8	12 ± 4	0.11 ± 0.04	27 ± 2
3	1.8	5 ± 1	0.10 ± 0.02	28.8 ± 0.6
4	1.8	14 ± 5	0.14 ± 0.05	26 ± 1
5	1.8	9 ± 2	0.07 ± 0.02	24 ± 1
6	1.8	3.8 ± 0.9	0.07 ± 0.02	25 ± 1

Table 1.3. Best Fit Parameters for Li and Draine Model

Region	Average β	Total Mass $[10^5 M_\odot]$	Surface Density $[M_\odot pc^{-2}]$	Average Temperature [K]
1	2.0	219 ± 103	0.4 ± 0.2	24 ± 2
2	2.0	54 ± 19	0.5 ± 0.2	25 ± 1
3	2.0	26 ± 5	0.48 ± 0.09	26.4 ± 0.5
4	2.0	67 ± 23	0.7 ± 0.2	24.4 ± 0.8
5	2.0	40 ± 9	0.33 ± 0.07	22.4 ± 0.9
6	2.0	17 ± 4	0.32 ± 0.08	23.5 ± 0.9

Table 1.4. Best Fit Parameters for β As A Free Parameter

Region	Average β	Total Mass $[M_\odot]$	Surface Density $[10^5 M_\odot pc^{-2}]$	Average Temperature [K]
1	2.2 ± 0.2	73 ± 35	0.14 ± 0.06	22 ± 1
2	2.3 ± 0.2	19 ± 6	0.18 ± 0.05	22 ± 2
3	2.34 ± 0.09	9 ± 1	0.18 ± 0.02	23.0 ± 0.9
4	2.2 ± 0.1	22 ± 6	0.21 ± 0.05	22 ± 1
5	2.1 ± 0.2	12 ± 4	0.10 ± 0.03	22 ± 1
6	2.1 ± 0.1	5 ± 1	0.09 ± 0.02	23.0 ± 0.9

The wellness of each fit is shown figures 3.3, 3.4, and 3.5 for the Plank model, Li and Draine model, and beta as a free parameter respectively. The quality of the fit is determined by how well the expected flux from the SED fitting matches the observed flux. If the fits are able to recreate the observed emission, then all of the points will lie on the line $y = x$ shown in the plots as a black line. If the SED is underestimating the flux, the points will appear below the 1 to 1 line, and an over estimation from the SED will result in points above the line.

Using these plots, it is clear that the SED is over estimating the 450μm flux despite the care taken while accounting for the odd beam shape of the 450μm data. This overestimation was not a result of a poor fit, but rather a calibration error in the 450μm observations. The intrinsic error to the SCUBA-2 450μm data was determined by extrapolating an expected value from the 350μm and 500μm KINGFISH data assuming the decrease in intensity was linear. In order to avoid any errors in our final parameter maps, we substitute the 450μm emission with KINGFISH 500μm emission. The quality of fit maps using the 500μm emission are shown in figures 3.6, 3.7, and 3.8 for the Planck model, Li and Draine model and the emissivity as a free parameter respectively. To assign a numerical quantity to the vertical distance was calculated for each point to the 1 to 1 line and then summed. The summed distances are shown in table 3.5 and suggest the best fit comes from allowing the emissivity index to vary.

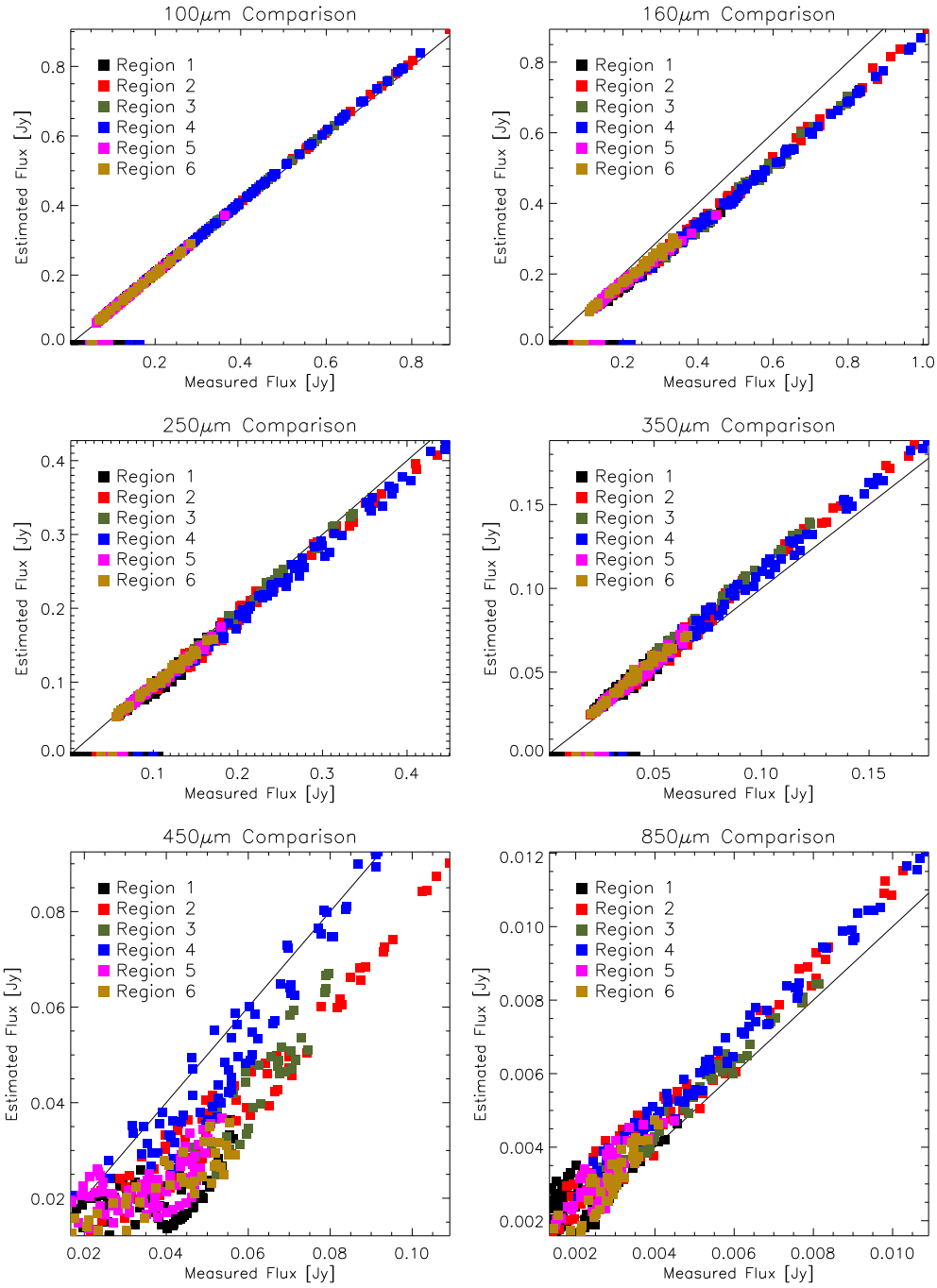

Figure 1.3: Quality of the SED fits to the Planck model using the 450μm emission. The regions shown are the regions in figure 3.1.

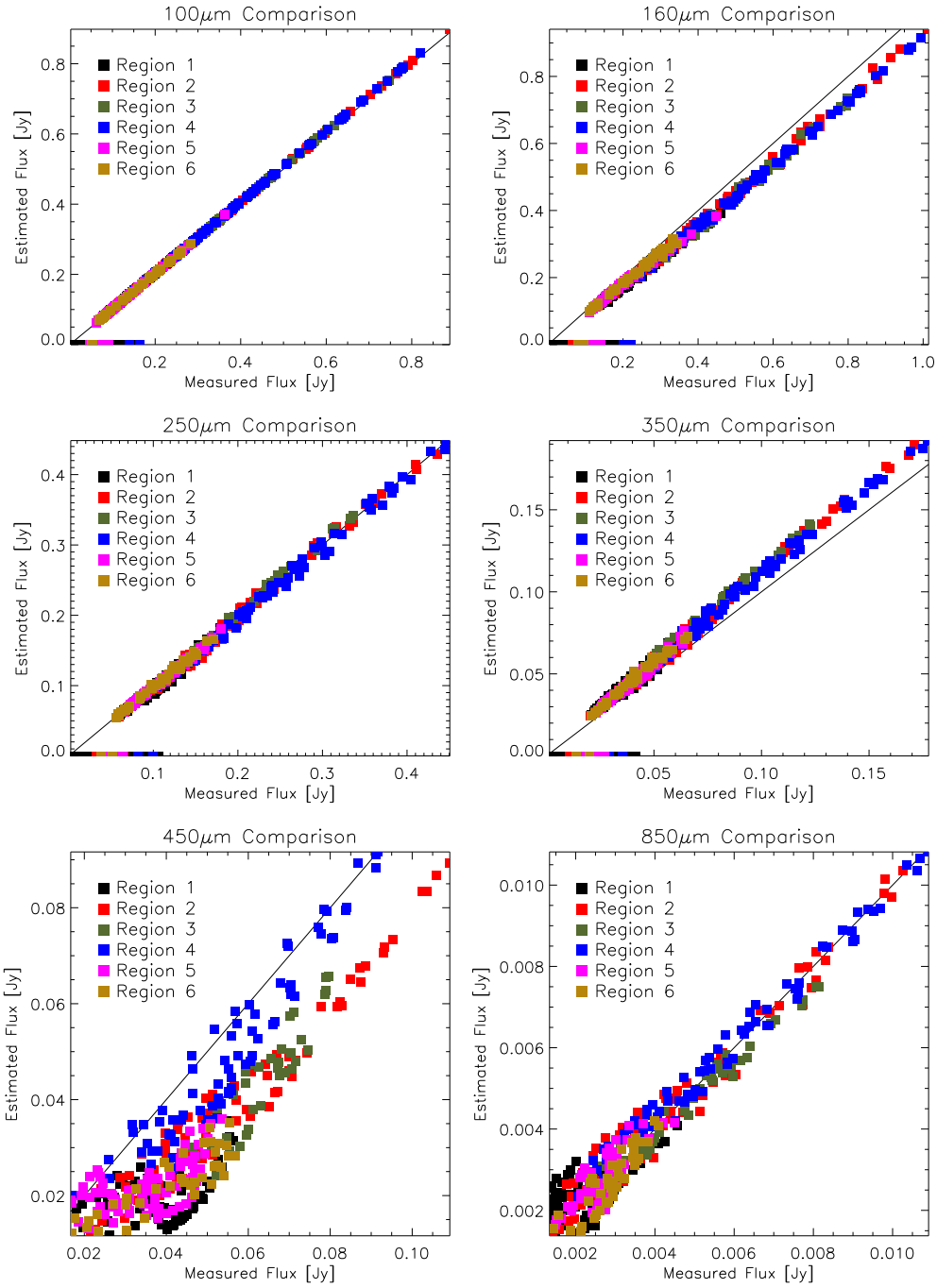

Figure 1.4: Quality of the SED fits to the Li and Draine model using the 450μm emission. The regions shown are the regions in figure 3.1.

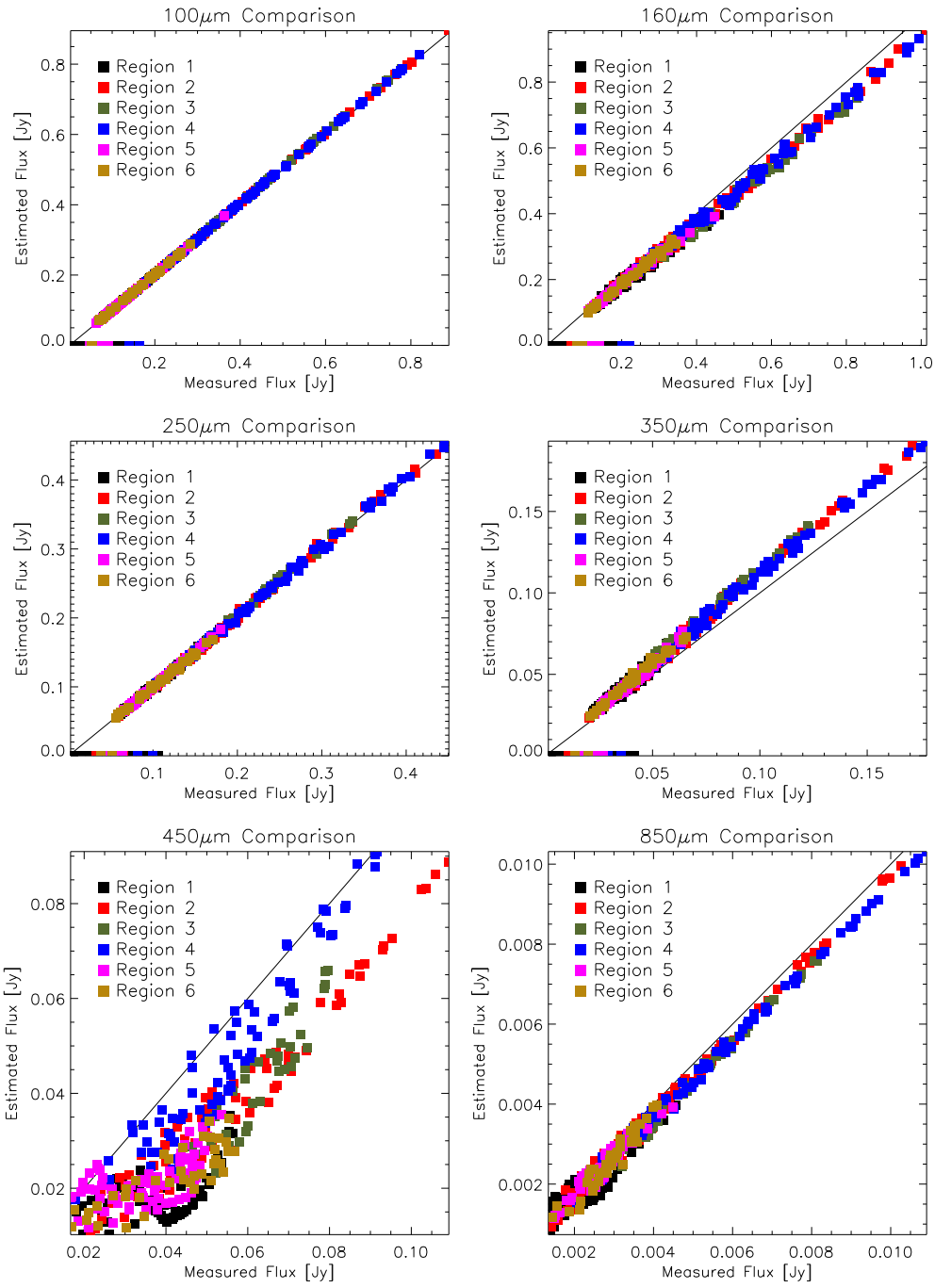

Figure 1.5: Quality of the SED fits with the dust emissivity index as a free parameter using the 450μm emission. The regions shown are the regions in figure 3.1.

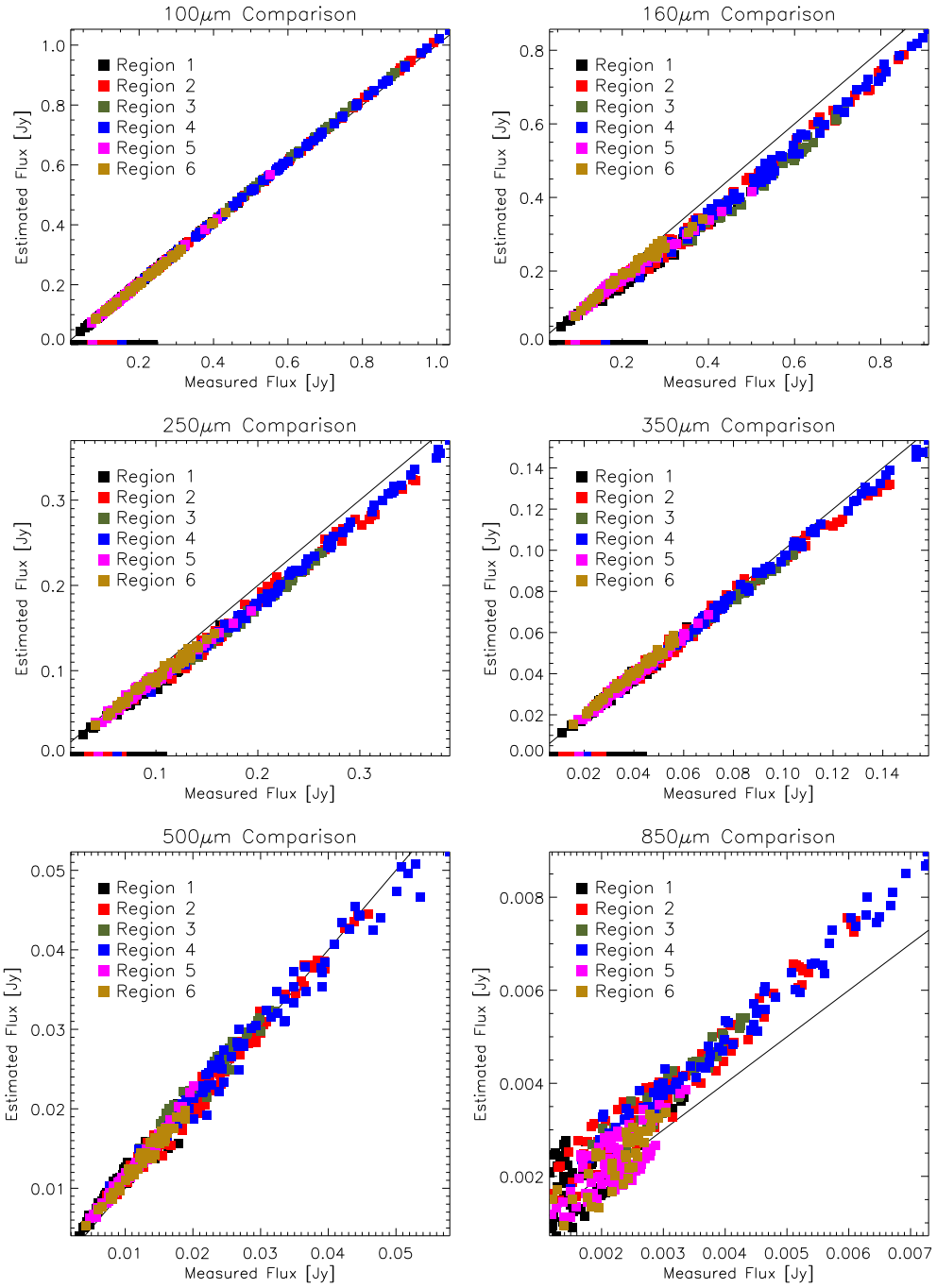

Figure 1.6: Quality of the SED fits using to the Planck model with the 500μm emission. The regions shown are the regions in figure 3.1.

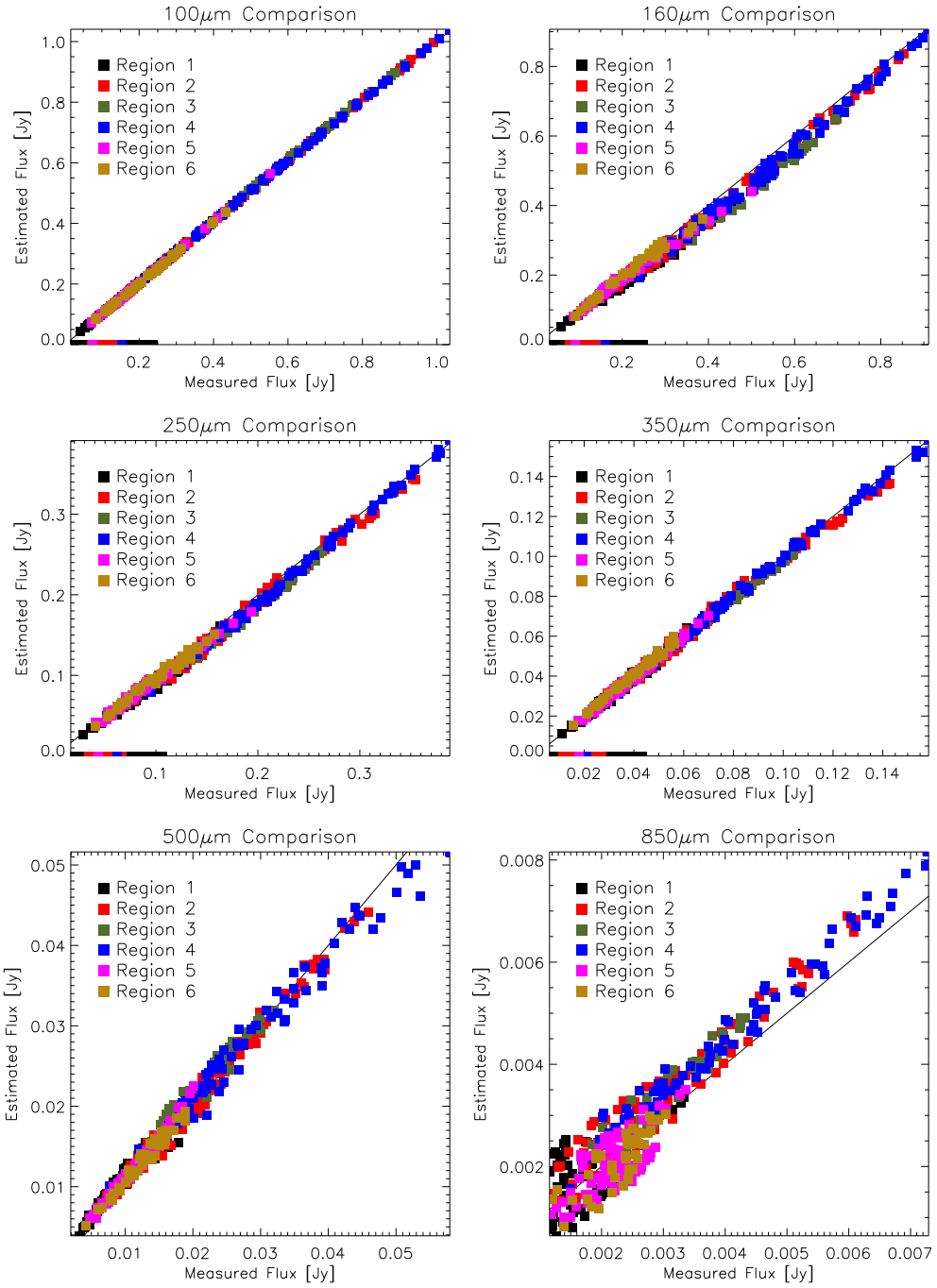

Figure 1.7: Quality of the SED fits using the Planck model with the 500μm emission. The regions shown are the regions in figure 3.1.

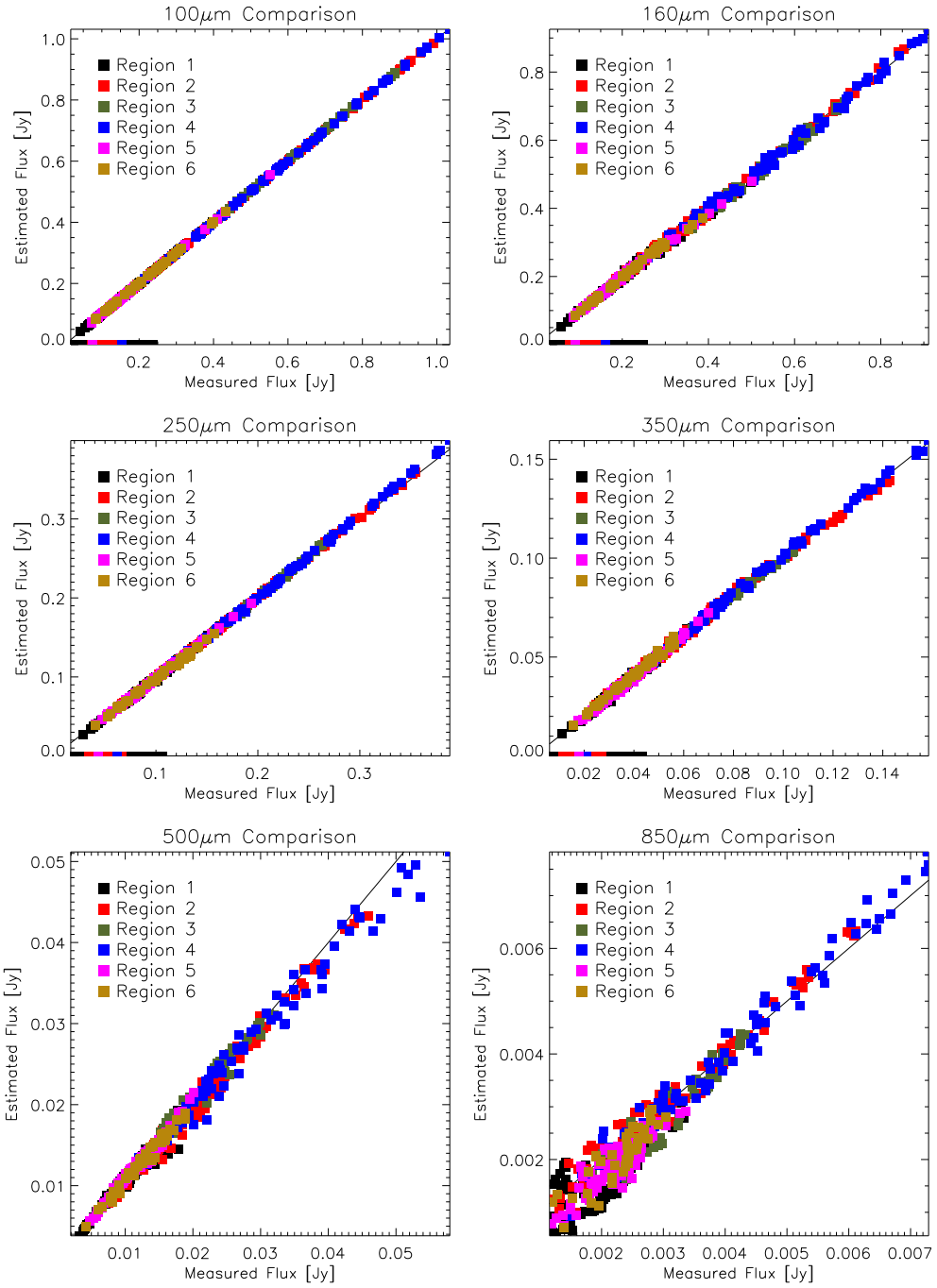

Figure 1.8: Quality of the SED fits with the emissivity index as a free paramter with the 500μm emission. The regions shown are the regions in figure 3.1.

Table 1.5. Total Distance to 1 to 1 Line

Observation	Planck Model	Li and Draine Model	Variable Emissivity Index
100μm	0.000	0.01245	01277
160μm	15.55	8.979	2.159
250μm	5.808	3.072	0.4465
350μm	0.8045	0.3541	0.1161
500μm	0.02825	0.05218	0.09528
Total	23.01	12.58	3.131

1.2.2 Total Region Flux SED Fits

The second method used to determine the dust mass, was to fit the SED to the flux of each region in figure 3.1. Performing the fit in this manner is beneficial because it increases the signal to noise of the region and produces a more precise set of parameters. Initially, this style of fit was carried in the same fashion as the individual pixel fits by fixing the emissivity index to 1.8 and 2.0, and allowing the emissivity index to vary. However, given the greater range of mass values for the region fits, a single valued initial condition for the mass would produce a set of parameters that did not converge to the absolute minimum. The dependence of the initial mass and the converged parameter with a variable emissivity index are shown in figure 3.9. Similarly, if we fix the emissivity index, the dependence on the initial mass is nonexistent until the Levinberg-Marquardt method is unable to converge to an appropriate fit, figure 3.10.

Since we can't let emissivity index vary freely, an alternative method to determine it's value needs to be implemented. The emissivity index was de-

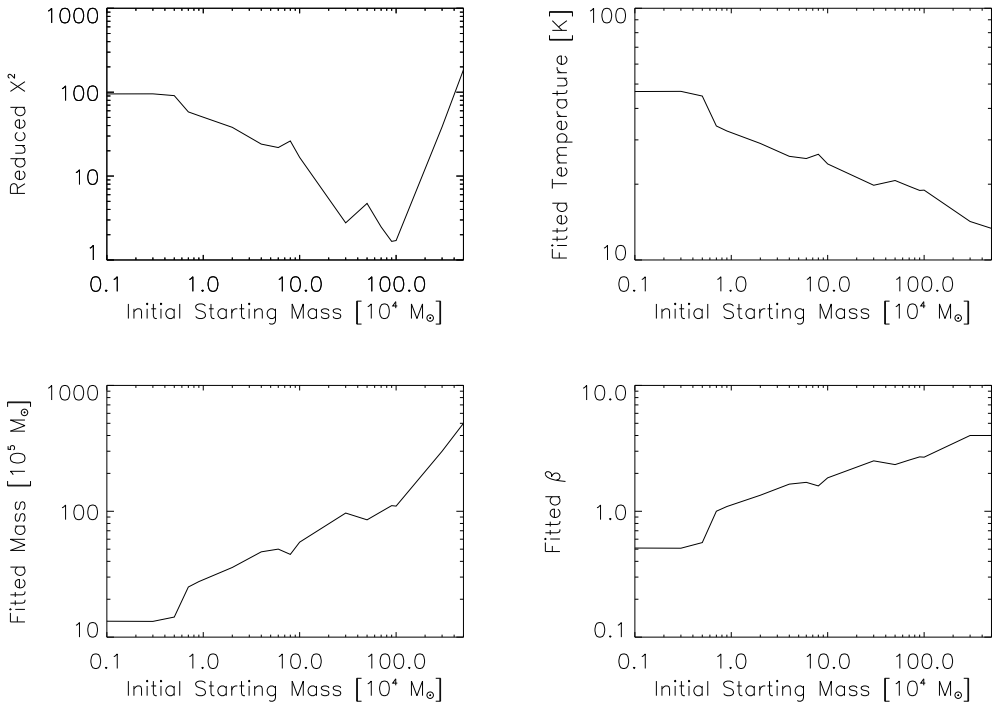

Figure 1.9: Returned SED fitting output with Planck opacity for the χ^2, temperature, mass, and emissivity index with varying initial conditions. The top left panels shows the χ^2 values for each starting mass. The top right, bottom left, and bottom right panels show the returned temperatures, mass, and emissivity index.

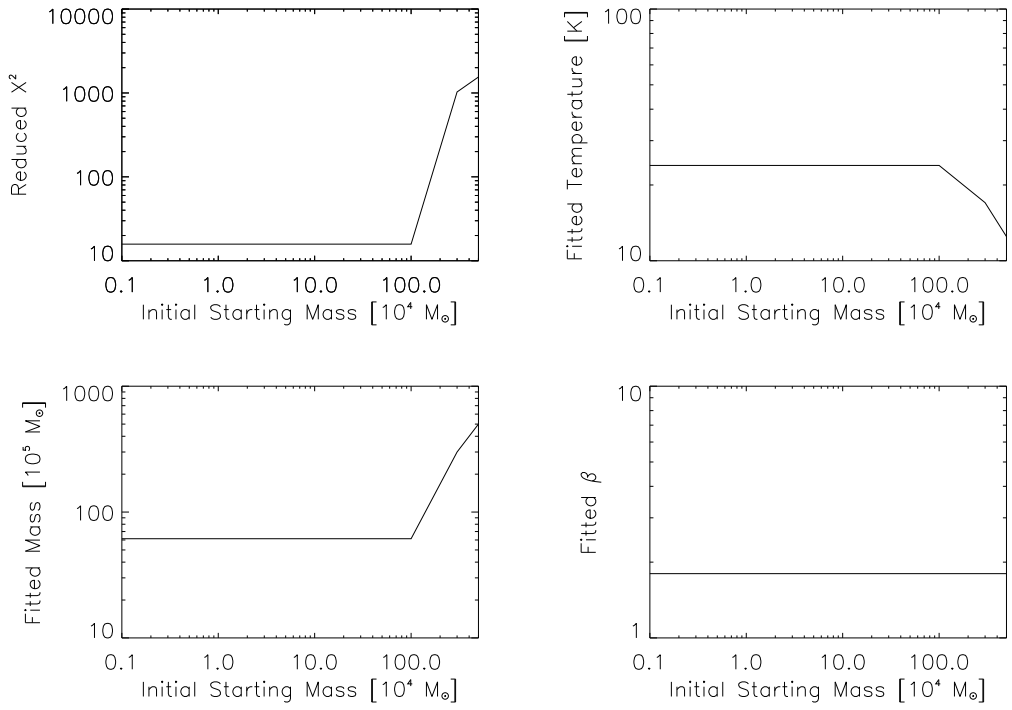

Figure 1.10: The same as figure 3.9, however the emissivity index has been fixed to 1.8.

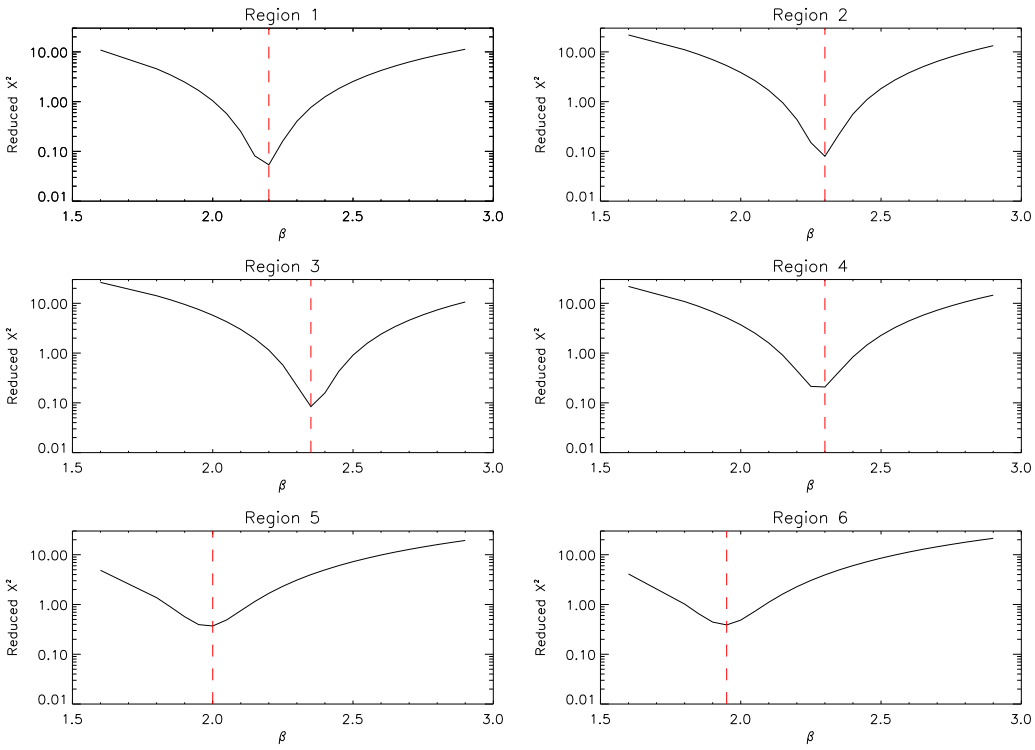

Figure 1.11: Plots for each region from figure 3.1 showing the fixed emissivity index value and the resulting reduced χ^2 value.

termined by fixing it over a range of 1.6 to 2.9 with a spacing of 0.05. The best emissivity index is determined by which value returns the lowest reduced χ^2. Plots showing the behavior of the χ^2 values with each emissivity index value are shown in figure 3.11 where the best value selected is represented by the red line. The results of each region using the fixed emissivity indices are shown in table 3.6, and their resulting SED's are shown in figure 3.12.

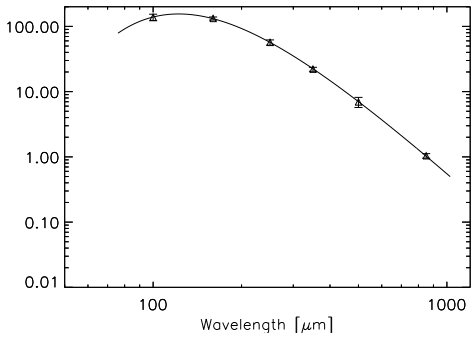

(a) Region 1 SED

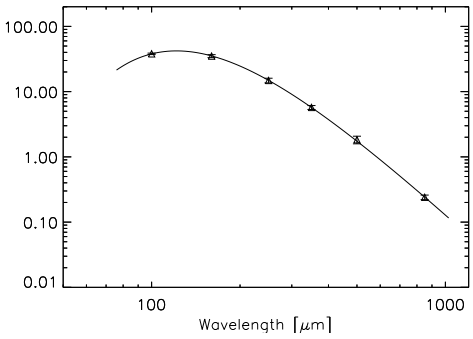

(b) Region 2 SED

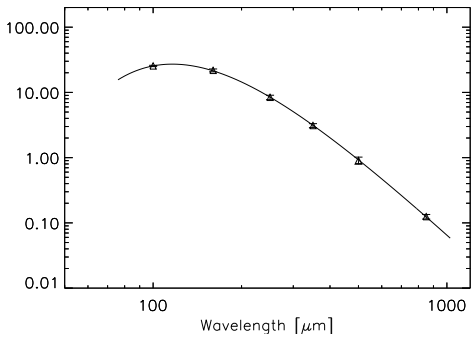

(c) Region 3 SED

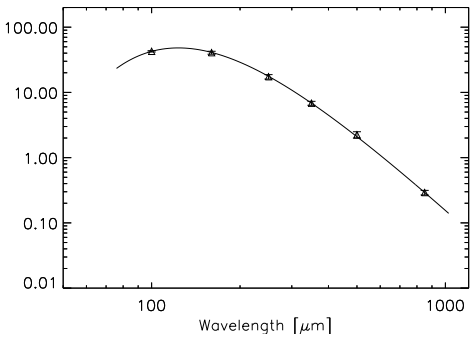

(d) Region 4 SED

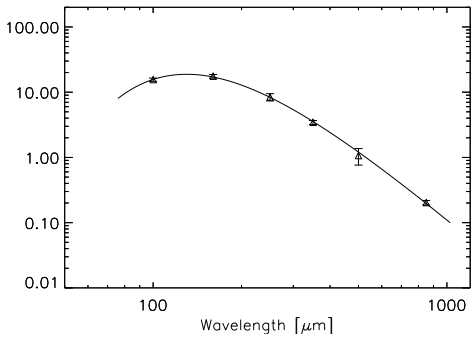

(e) Region 5 SED

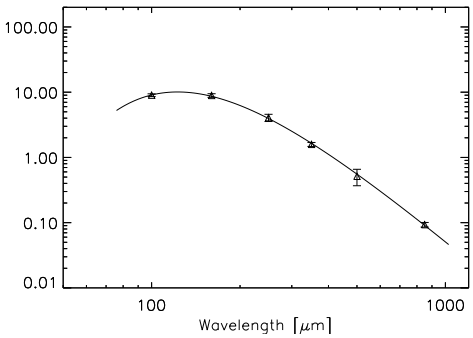

(f) Region 6 SED

Figure 1.12: SED fits for the flux of each region in figure 3.1 using the Planck Opacity.

Table 1.6. Best Fit Parameters for Planck Opacity

Region	Average β	Total Mass $[10^5 M_\odot]$	Surface Density $[M_\odot pc^{-2}]$	Average Temperature [K]
1	2.20 ± 0.03	70 ± 6	0.14 ± 0.01	22.8 ± 0.5
2	2.30 ± 0.03	19 ± 1	0.18 ± 0.01	22.5 ± 0.3
3	2.35 ± 0.03	9.6 ± 0.6	0.18 ± 0.01	23.3 ± 0.3
4	2.30 ± 0.03	23 ± 1	0.22 ± 0.01	22.2 ± 0.2
5	2.00 ± 0.03	11.3 ± 0.8	0.092 ± 0.007	22.3 ± 0.4
6	1.95 ± 0.03	4.5 ± 0.3	0.084 ± 0.006	23.9 ± 0.4

1.3 Discussion

1.3.1 Reliability of Individual Pixel Fits

The issue on whether or not the individual pixel fits are reliable is raised after seeing a strong dependence with the initial mass of the region SED fits shown in figure 3.9. Since any dependence on the initial mass has been removed in the global region fits, an agreement between the total pixel mass and the region fits would suggest that the initial mass used in the pixel fitting is an appropriate value. This is further strengthened by the smaller mass range of pixel fits. The smaller range allows the fitting method to hone into a smaller area of the χ^2 space avoiding any possible local minima to converge on.

1.3.2 Comparison with Previous Work

We can check the validity of our results by comparing them to previous SED fits using the KINGFISH data (Galametz et al., 2012). The best fit parameters from their fitting was T=20.2K±4K and β=2.3±0.2 which agree within error to our results of T=22K±1K and β=2.2±0.2 for a variable emissivity index. To test agreement with our mass we need to take into account several factors. The first being a lessened flux from the extended structure removal, and the second is the selection of the opacity value. Their reported mass for a variable emissivity index reported by Galametz et al. (2012) was $782^{+80}_{-66}\times10^5 M_\odot$ for the sum of pixels in the parameter maps. We can scale the mass values by finding the ratio $\kappa_{Galametz}$ over κ_{Ours} which comes out to be 0.342. If we then scale by the amount of flux removed in the extended structure removal, we can scale the mass to $175^{+19}_{-17}\times10^5 M_\odot$ which is above our maximum value of $108\times10^5 M_\odot$. This discrepancy can likely be attributed to how the total mass was found in each method. For our method we use the mass returned from fitting, and in Galametz et al. (2012) they use equation 3.4 using the 500μm emission to determine a dust mass.

1.3.3 Effects of 850μm Emission

The major difference between our work on NGC3627 and the work done in Galametz et al. (2012) is the presence of the 850μm data point. In our analysis the presence of the 850μm has shown little effect on the returned parameters. The returned values for a variable emissivity index are shown in table 3.7.

Table 1.7. Best Fit Parameters Excluding 850μm Emission

Region	Average β	Total Mass $[10^5 M_\odot]$	Surface Density $[M_\odot pc^{-2}]$	Average Temperature [K]
1	2.3 ± 0.3	75 ± 29	0.15 ± 0.06	22 ± 2
2	2.3 ± 0.3	18 ± 5	0.17 ± 0.05	23 ± 2
3	2.4 ± 0.2	10 ± 1	0.19 ± 0.02	23 ± 1
4	2.2 ± 0.2	22 ± 5	0.21 ± 0.05	23 ± 2
5	2.3 ± 0.2	13 ± 3	0.11 ± 0.03	21 ± 1
6	2.2 ± 0.2	5 ± 1	0.10 ± 0.02	22 ± 1

The absence of a significant change in the returned parameters is indicative of a lack of any excess submillimeter emission suggestive of an abundance of a very cold (T $\lesssim$ 10K) dust component (Dale et al., 2012). This excess in emission is typically seen in low-metalicity systems such as dwarf galaxies (Madden et al., 2011), but has also been seen in NGC3627 (Galametz et al., 2014). While our results show no excess of emission at 850μm (evident in figures 3.6, 3.7, and 3.8), we should not expect to see any submillimeter excess given the log(O/H) + 12 is either 8.34 or 8.99 depending on the calibration values used (Moustakas et al., 2010).

Bibliography

Abel, T., Anninos, P., Zhang, Y., & Norman, M. L. 1997, New A, 2, 181

Burden, R. L. & Faires, J. D. 2001, Numerical analysis

Chapin, E. L., Berry, D. S., Gibb, A. G., Jenness, T., Scott, D., Tilanus, R. P. J., Economou, F., & Holland, W. S. 2013, MNRAS, 430, 2545

Dale, D. A., Aniano, G., Engelbracht, C. W., Hinz, J. L., Krause, O., Montiel, E. J., Roussel, H., Appleton, P. N., Armus, L., Beirão, P., Bolatto, A. D., Brandl, B. R., Calzetti, D., Crocker, A. F., Croxall, K. V., Draine, B. T., Galametz, M., Gordon, K. D., Groves, B. A., Hao, C.-N., Helou, G., Hunt, L. K., Johnson, B. D., Kennicutt, R. C., Koda, J., Leroy, A. K., Li, Y., Meidt, S. E., Miller, A. E., Murphy, E. J., Rahman, N., Rix, H.-W., Sandstrom, K. M., Sauvage, M., Schinnerer, E., Skibba, R. A., Smith, J.-D. T., Tabatabaei, F. S., Walter, F., Wilson, C. D., Wolfire, M. G., & Zibetti, S. 2012, ApJ, 745, 95

Dempsey, J. T., Friberg, P., Jenness, T., Tilanus, R. P. J., Thomas, H. S., Holland, W. S., Bintley, D., Berry, D. S., Chapin, E. L., Chrysostomou, A., Davis, G. R., Gibb, A. G., Parsons, H., & Robson, E. I. 2013, MNRAS, 430, 2534

Dobbs, C. L., Krumholz, M. R., Ballesteros-Paredes, J., Bolatto, A. D., Fukui, Y., Heyer, M., Mac Low, M.-M., Ostriker, E. C., & Vázquez-Semadeni, E. 2013, ArXiv e-prints

Drabek, E., Hatchell, J., Friberg, P., Richer, J., Graves, S., Buckle, J. V., Nutter, D., Johnstone, D., & Di Francesco, J. 2012, MNRAS, 426, 23

Draine, B. T. 2011, Physics of the Interstellar and Intergalactic Medium

Elmegreen, B. G. 1987, ApJ, 312, 626

Field, G. B. & Saslaw, W. C. 1965, ApJ, 142, 568

Galametz, M., Albrecht, M., Kennicutt, R., Aniano, G., Bertoldi, F., Calzetti, D., Croxall, K. V., Dale, D., Draine, B., Engelbracht, C., Gordon, K., Hinz, J., Hunt, L. K., Kirkpatrick, A., Murphy, E., Roussel, H., Skibba, R. A., Walter, F., Weiss, A., & Wilson, C. D. 2014, MNRAS, 439, 2542

Galametz, M., Kennicutt, R. C., Albrecht, M., Aniano, G., Armus, L., Bertoldi, F., Calzetti, D., Crocker, A. F., Croxall, K. V., Dale, D. A., Donovan Meyer, J., Draine, B. T., Engelbracht, C. W., Hinz, J. L., Roussel, H., Skibba, R. A., Tabatabaei, F. S., Walter, F., Weiss, A., Wilson, C. D., & Wolfire, M. G. 2012, MNRAS, 425, 763

Gavin, H. P. 2013, The Levenberg-Marquardt method for nonlinear least squares curve-fitting problems, Tech. rep., Department of Civil and Environmental Engineering, Duke University

Glover, S. C. O. 2003, ApJ, 584, 331

Gould, R. J. & Salpeter, E. E. 1963, ApJ, 138, 393

Gry, C., Boulanger, F., Nehmé, C., Pineau des Forêts, G., Habart, E., & Falgarone, E. 2002, A&A, 391, 675

Herbst, E., Chang, Q., & Cuppen, H. M. 2005, Journal of Physics Conference Series, 6, 18

Holland, W. S., Bintley, D., Chapin, E. L., Chrysostomou, A., Davis, G. R., Dempsey, J. T., Duncan, W. D., Fich, M., Friberg, P., Halpern, M., Irwin, K. D., Jenness, T., Kelly, B. D., MacIntosh, M. J., Robson, E. I., Scott, D., Ade, P. A. R., Atad-Ettedgui, E., Berry, D. S., Craig, S. C., Gao, X., Gibb, A. G., Hilton, G. C., Hollister, M. I., Kycia, J. B., Lunney, D. W., McGregor, H., Montgomery, D., Parkes, W., Tilanus, R. P. J., Ullom, J. N., Walther, C. A., Walton, A. J., Woodcraft, A. L., Amiri, M., Atkinson, D., Burger, B., Chuter, T., Coulson, I. M., Doriese, W. B., Dunare, C., Economou, F., Niemack, M. D., Parsons, H. A. L., Reintsema, C. D., Sibthorpe, B., Smail, I., Sudiwala, R., & Thomas, H. S. 2013, MNRAS, 430, 2513

Jura, M. 1975, ApJ, 197, 575

Kennicutt, R. C., Calzetti, D., Aniano, G., Appleton, P., Armus, L., Beirão, P., Bolatto, A. D., Brandl, B., Crocker, A., Croxall, K., Dale, D. A., Meyer, J. D., Draine, B. T., Engelbracht, C. W., Galametz, M., Gordon, K. D., Groves, B., Hao, C.-N., Helou, G., Hinz, J., Hunt, L. K., Johnson, B., Koda, J., Krause, O., Leroy, A. K., Li, Y., Meidt, S., Montiel, E., Murphy, E. J., Rahman, N., Rix, H.-W., Roussel, H., Sandstrom, K., Sauvage, M.,

Schinnerer, E., Skibba, R., Smith, J. D. T., Srinivasan, S., Vigroux, L., Walter, F., Wilson, C. D., Wolfire, M., & Zibetti, S. 2011, PASP, 123, 1347

Kennicutt, R. C. & Evans, N. J. 2012, ARA&A, 50, 531

Kennicutt, Jr., R. C., Armus, L., Bendo, G., Calzetti, D., Dale, D. A., Draine, B. T., Engelbracht, C. W., Gordon, K. D., Grauer, A. D., Helou, G., Hollenbach, D. J., Jarrett, T. H., Kewley, L. J., Leitherer, C., Li, A., Malhotra, S., Regan, M. W., Rieke, G. H., Rieke, M. J., Roussel, H., Smith, J.-D. T., Thornley, M. D., & Walter, F. 2003, PASP, 115, 928

Kim, W.-T. & Ostriker, E. C. 2001, ApJ, 559, 70

Krumholz, M. R. 2014, ArXiv e-prints

Kuno, N., Sato, N., Nakanishi, H., Hirota, A., Tosaki, T., Shioya, Y., Sorai, K., Nakai, N., Nishiyama, K., & Vila-Vilaró, B. 2007, PASJ, 59, 117

Kwan, J. 1979, ApJ, 229, 567

Leroy, A. K., Walter, F., Bigiel, F., Usero, A., Weiss, A., Brinks, E., de Blok, W. J. G., Kennicutt, R. C., Schuster, K.-F., Kramer, C., Wiesemeyer, H. W., & Roussel, H. 2009, AJ, 137, 4670

Li, A. & Draine, B. T. 2001, ApJ, 554, 778

Madden, S. C., Galametz, M., Cormier, D., Lebouteiller, V., Galliano, F., Hony, S., Rémy, A., Sauvage, M., Contursi, A., Sturm, E., Poglitsch, A., Pohlen, M., Smith, M. W. L., Bendo, G., & O'Halloran, B. 2011, in EAS Publications Series, Vol. 52, EAS Publications Series, ed. M. Röllig, R. Simon, V. Ossenkopf, & J. Stutzki, 95–101

Markwardt, C. B. 2009, in Astronomical Society of the Pacific Conference Series, Vol. 411, Astronomical Data Analysis Software and Systems XVIII, ed. D. A. Bohlender, D. Durand, & P. Dowler, 251

McKee, C. F. & Ostriker, E. C. 2007, ARA&A, 45, 565

Moustakas, J., Kennicutt, Jr., R. C., Tremonti, C. A., Dale, D. A., Smith, J.-D. T., & Calzetti, D. 2010, ApJS, 190, 233

Palla, F., Salpeter, E. E., & Stahler, S. W. 1983, ApJ, 271, 632

Parker, E. N. 1966, ApJ, 145, 811

Pirronello, V., Liu, C., Shen, L., & Vidali, G. 1997, ApJ, 475, L69

Planck Collaboration, Abergel, A., Ade, P. A. R., Aghanim, N., Arnaud, M., Ashdown, M., Aumont, J., Baccigalupi, C., Balbi, A., Banday, A. J., Barreiro, R. B., Bartlett, J. G., Battaner, E., Benabed, K., Benoît, A., Bernard, J.-P., Bersanelli, M., Bhatia, R., Bock, J. J., Bonaldi, A., Bond, J. R., Borrill, J., Bouchet, F. R., Boulanger, F., Bucher, M., Burigana, C., Cabella, P., Cardoso, J.-F., Catalano, A., Cayón, L., Challinor, A., Chamballu, A., Chiang, L.-Y., Chiang, C., Christensen, P. R., Clements, D. L., Colombi, S., Couchot, F., Coulais, A., Crill, B. P., Cuttaia, F., Danese, L., Davies, R. D., Davis, R. J., de Bernardis, P., de Gasperis, G., de Rosa, A., de Zotti, G., Delabrouille, J., Delouis, J.-M., Désert, F.-X., Dickinson, C., Dobashi, K., Donzelli, S., Doré, O., Dörl, U., Douspis, M., Dupac, X., Efstathiou, G., Enßlin, T. A., Eriksen, H. K., Finelli, F., Forni, O., Frailis, M., Franceschi, E., Galeotta, S., Ganga, K., Giard, M., Giardino, G., Giraud-Héraud, Y., González-Nuevo, J., Górski, K. M., Gratton, S., Gregorio, A., Gruppuso,

A., Guillet, V., Hansen, F. K., Harrison, D., Henrot-Versillé, S., Herranz, D., Hildebrandt, S. R., Hivon, E., Hobson, M., Holmes, W. A., Hovest, W., Hoyland, R. J., Huffenberger, K. M., Jaffe, A. H., Jones, A., Jones, W. C., Juvela, M., Keihänen, E., Keskitalo, R., Kisner, T. S., Kneissl, R., Knox, L., Kurki-Suonio, H., Lagache, G., Lamarre, J.-M., Lasenby, A., Laureijs, R. J., Lawrence, C. R., Leach, S., Leonardi, R., Leroy, C., Linden-Vørnle, M., López-Caniego, M., Lubin, P. M., Macías-Pérez, J. F., MacTavish, C. J., Maffei, B., Mandolesi, N., Mann, R., Maris, M., Marshall, D. J., Martin, P., Martínez-González, E., Masi, S., Matarrese, S., Matthai, F., Mazzotta, P., McGehee, P., Meinhold, P. R., Melchiorri, A., Mendes, L., Mennella, A., Mitra, S., Miville-Deschênes, M.-A., Moneti, A., Montier, L., Morgante, G., Mortlock, D., Munshi, D., Murphy, A., Naselsky, P., Natoli, P., Netterfield, C. B., Nørgaard-Nielsen, H. U., Noviello, F., Novikov, D., Novikov, I., Osborne, S., Pajot, F., Paladini, R., Pasian, F., Patanchon, G., Perdereau, O., Perotto, L., Perrotta, F., Piacentini, F., Piat, M., Plaszczynski, S., Pointecouteau, E., Polenta, G., Ponthieu, N., Poutanen, T., Prézeau, G., Prunet, S., Puget, J.-L., Reach, W. T., Rebolo, R., Reinecke, M., Renault, C., Ricciardi, S., Riller, T., Ristorcelli, I., Rocha, G., Rosset, C., Rubiño-Martín, J. A., Rusholme, B., Sandri, M., Santos, D., Savini, G., Scott, D., Seiffert, M. D., Shellard, P., Smoot, G. F., Starck, J.-L., Stivoli, F., Stolyarov, V., Sudiwala, R., Sygnet, J.-F., Tauber, J. A., Terenzi, L., Toffolatti, L., Tomasi, M., Torre, J.-P., Tristram, M., Tuovinen, J., Umana, G., Valenziano, L., Verstraete, L., Vielva, P., Villa, F., Vittorio, N., Wade, L. A., Wandelt, B. D., Yvon, D., Zacchei, A., & Zonca, A. 2011, A&A, 536, A25

Reuter, H.-P., Sievers, A. W., Pohl, M., Lesch, H., & Wielebinski, R. 1996, A&A, 306, 721

Walter, F., Brinks, E., de Blok, W. J. G., Bigiel, F., Kennicutt, Jr., R. C., Thornley, M. D., & Leroy, A. 2008, AJ, 136, 2563

Wilson, C. D., Warren, B. E., Israel, F. P., Serjeant, S., Attewell, D., Bendo, G. J., Butner, H. M., Chanial, P., Clements, D. L., Golding, J., Heesen, V., Irwin, J., Leech, J., Matthews, H. E., Mühle, S., Mortier, A. M. J., Petitpas, G., Sánchez-Gallego, J. R., Sinukoff, E., Shorten, K., Tan, B. K., Tilanus, R. P. J., Usero, A., Vaccari, M., Wiegert, T., Zhu, M., Alexander, D. M., Alexander, P., Azimlu, M., Barmby, P., Brar, R., Bridge, C., Brinks, E., Brooks, S., Coppin, K., Côté, S., Côté, P., Courteau, S., Davies, J., Eales, S., Fich, M., Hudson, M., Hughes, D. H., Ivison, R. J., Knapen, J. H., Page, M., Parkin, T. J., Rigopoulou, D., Rosolowsky, E., Seaquist, E. R., Spekkens, K., Tanvir, N., van der Hulst, J. M., van der Werf, P., Vlahakis, C., Webb, T. M., Weferling, B., & White, G. J. 2012, MNRAS, 424, 3050

Wolfire, M. G., McKee, C. F., Hollenbach, D., & Tielens, A. G. G. M. 2003, ApJ, 587, 278

Wolfire, M. G., Tielens, A. G. G. M., Hollenbach, D., & Kaufman, M. J. 2008, ApJ, 680, 384